Effective heating to several thousand kelvins of an optically trapped sphere in a liquid

Ignacio A. Martínez,[1] Édgar Roldán,[2] Juan M. R. Parrondo,[2] and Dmitri Petrov[3,4,*]

[1]*ICFO - Institut de Ciències Fotòniques, Mediterranean Technology Park, Av. Carl Friedrich Gauss, num. 3, 08860 Castelldefels (Barcelona), Spain*

[2]*Departamento de Física Atómica, Molecular y Nuclear and GISC, Universidad Complutense de Madrid, 28040 Madrid, Spain*

[3]*ICFO - Institut de Ciències Fotòniques, Mediterranean Technology Park, 08860 Castelldefels (Barcelona), Spain*

[4]*ICREA - Institucio Catalana de Recerca i Estudis Avancats, Barcelona, Spain*

(Received 4 September 2012; revised manuscript received 10 January 2013; published 25 March 2013)

The cooling of the center of mass motion of optically trapped microspheres by feedback stabilization is advancing rapidly, and cooling below several millikelvin is possible. Such a controllable attenuation of the motion is an important step towards new experiments in different areas of physics. In this study we suggest going in the opposite direction, in controlling the motion of optically trapped spheres, namely, to increase the amplitude of their Brownian fluctuations. We show that the effective kinetic temperature of a Brownian particle may achieve 3000 K when an additional external random force is applied to the sphere. We demonstrate experimentally how the temperature increase affects the histogram of the position of the Brownian particle, its power spectral density, its response to an external perturbation, and the statistics of the Kramers transitions in a double-well potential. Effects related to the nonideal character of the white noise generated experimentally are also analyzed. This experimental technique allows tuning and controlling the kinetic temperature of the sphere with millisecond resolution over a wide range and along a single spatial direction, and has considerable potential for the study of thermodynamic processes at the microscopic scale.

DOI: 10.1103/PhysRevE.87.032159 PACS number(s): 05.40.Jc, 05.20.−y, 82.70.Dd, 87.80.Cc

I. INTRODUCTION

Since the first of Ashkin's experiments [1], where the feedback stabilization of optically trapped particles was suggested, the cooling of the center of mass motion of optically trapped microspheres has advanced rapidly, and now cooling below several millikelvin has become possible [2,3]. Such a controllable attenuation of the motion is an important step towards new experiments in different areas of physics. In this study we suggest going in the opposite direction, namely, to increase their Brownian fluctuations in a controllable way.

The Brownian motion of microspheres in liquid has offered a model system for experimental studies of processes where thermal fluctuations are important. Out of equilibrium processes in biophysics and colloidal systems [4–6], Kramers transitions [7], and a micrometer-sized stochastic engine [8] are just several examples of such processes. We present an experimental technique that allows increasing the amplitude of the Brownian fluctuations in a controllable way with millisecond response time, significantly extending the range of the parameters used in modeling equilibrium and out of equilibrium processes. No sources of heat, such as optical beams or micro ovens, are required.

Both the temperature T of the thermal bath and its viscous friction coefficient γ affect the amplitude of the Brownian fluctuations. We are not aware of methods allowing dynamic change of the viscosity; however, the temperature has been controlled by heating the Brownian sphere or its surroundings. Spherical colloids [9] or nanorods [10] were selectively heated by external sources of a light which is not absorbed by the solvent. In [8,11], the variation of the temperature in the surroundings of a dielectric sphere was achieved by an optical beam whose wavelength matches an absorption peak of the solvent. In aqueous experiments, the maximal temperature difference using the means described above is restricted by the evaporating and freezing temperatures of water. In all previous experiments the temperature increase did not exceed several tens of kelvin. The response time of several tens of milliseconds has been obtained due to the small volumes of the systems studied.

The fluctuations of the velocity and position are proportional to the kinetic temperature $T_{\rm kin}$, which for a free Brownian particle are equal to the temperature of the surrounding fluid T. Active optical feedback permits cooling down the kinetic temperature of optically trapped microspheres [2,3], and the same technique may increase the kinetic temperature if the active control is tuned to increase the sphere displacements. In this paper, we suggest an alternative and simpler method, based on combining an optical trap with a source of additional external forces acting on the trapped sphere. With our technique, we have achieved a situation where the Brownian sphere fluctuates in water in one of the directions with the center of mass motion corresponding to a temperature of several thousand kelvin, however, the viscous coefficient of the liquid and the temperature, describing the center of mass motion in two other directions, remain the same as for the temperature of the thermal bath.

Consider an overdamped Brownian particle in a fluid at temperature T. The particle is trapped in a harmonic potential of stiffness κ centered at x_0: $V(x) = \kappa(x - x_0)^2/2$. If an external force $\zeta(t)$ acts on the particle, then the position along the direction of the external force, $x(t)$, obeys the Langevin equation

$$\gamma \dot{x}(t) = -\kappa[x(t) - x_0] + \xi(t) + \zeta(t), \qquad (1)$$

*Corresponding author: dmitri.petrov@icfo.es

where $\xi(t)$ is a thermal force with a Gaussian white noise spectrum, zero mean, and correlation $\langle \xi(t)\xi(t')\rangle = 2k_B T\gamma\delta(t-t')$. Assume that the external force $\zeta(t)$ is also described by a stochastic process independent of the thermal noise, with zero mean and correlation $\langle \zeta(t)\zeta(t')\rangle = \sigma^2\Gamma(t-t')$, where $\Gamma(\tau)$ is a normalized function, $\int_{\mathbb{R}} \Gamma(\tau)\,d\tau = 1$, peaked at $\tau = 0$, and σ is the amplitude of the external noise. If the spectrum of external noise is white, i.e., $\Gamma(\tau) = \delta(\tau)$, then the particle is subject to an effective noise $\xi_{\text{eff}}(t) = \xi(t) + \zeta(t)$, with zero mean and correlation $\langle \xi_{\text{eff}}(t)\xi_{\text{eff}}(t')\rangle = 2k_B T_{\text{kin}}\gamma\delta(t-t')$, where

$$T_{\text{kin}} = T + \frac{\sigma^2}{2k_B\gamma}. \tag{2}$$

Hence the position of the particle along the x axis fluctuates corresponding to a kinetic temperature T_{kin} which is always higher than the temperature T of the thermal bath. Therefore, a stochastic force exerted on the sphere increases the kinetic temperature of the sphere without real heating of the surrounding fluid or the sphere. Notice also that the kinetic temperature along the axes perpendicular to the external force remains equal to T. The motion of the particle in the direction of the force is in every respect identical to the motion of a particle in a bath at temperature T_{kin} (this holds for underdamped particles as well). However, this is valid only if the external noise has a white noise power spectral density (PSD). Therefore, one of the goals of this paper is also to describe the limitations arising from the finite correlation time of the external noise, which are unavoidable in experimental realizations since the external force $\zeta(t)$ has a constant PSD only within some frequency range. Several experiments described in this paper used this technique and demonstrate its robustness and flexibility for several basic stochastic processes.

II. EXPERIMENTAL DETAILS

Various experimental techniques permit exerting controllable forces on an optically trapped sphere, either with magnetic [12] or optical [1–3] fields or by modulating the position of the trap $x_0(t)$ [13]. We have used random electric fields applied to optically trapped dielectric spheres with electric charges that remain constant, as we show below, during several thousand seconds. The setup includes the following principal parts shown and explained in Fig. 1.

Polystyrene microspheres (G. Kisker-Products for Biotechnology, http://www.kisker-biotech.com/, polystyrene microparticles PPs-1.0 with a diameter of 1.00 ± 0.05 μm) were diluted in distilled deionized water to a final concentration of a few spheres per milliliter.

The spheres were inserted into a custom-made electrophoretic fluid chamber with two electrodes connected to a computer controlled electric generator and an amplifier. The chamber was previously described in [14,15]. Electrical signals on the electrodes were produced by the generator fed with a noisy sequence close to white Gaussian noise. The sequence was generated using independent random variables $\zeta_{n\delta t}$, with $\langle \zeta_{n\delta t}\rangle = 0$, $\langle \zeta_{n\delta t}^2\rangle = A$, and $\langle \zeta_{n\delta t}\zeta_{m\delta t}\rangle = 0$ for $n \neq m$, A being the variance of the noise [16]. The time interval δt is the clock time of the generator, which is $\delta t = 0.2$ ms in the experiments. Notice that δt is a lower bound to the actual correlation time of the external force, which also depends on the response characteristics of the amplifier.

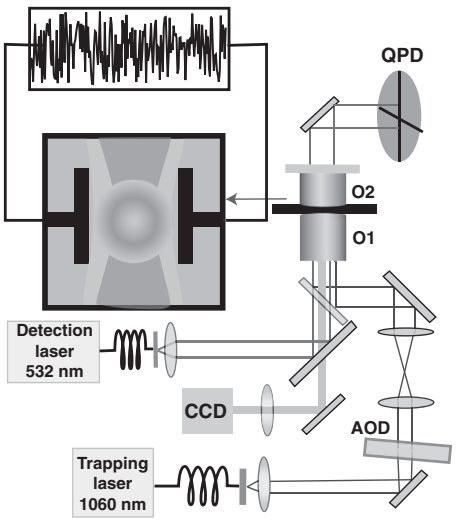

FIG. 1. Experimental setup. An acousto-optical deflector (AOD) (ISOMET LS55 NIR) steers a 1060 nm optical beam from a laser coupled into a single-mode fiber (ManLight, ML10-CW-P-OEM/TKS-OTS, maximal power 3 W). The AOD modulation voltage is obtained from an arbitrary waveform generator (Tabor Electronics WW1071) controlled by a LABVIEW program. The beam deflected by the AOD is expanded and inserted through an oil-immersed objective O1 (Nikon, CFI PL FL 100X NA 1.30) into a custom-made fluid chamber. An additional 532 nm optical beam from a laser coupled to a single-mode fiber (OZOptics) is collimated by a ($10\times$, NA = 0.10) microscope objective and passes through the trapping objective. The forward scattered detection beam is collected by a ($10\times$, NA = 0.10) microscope objective O2, and its back focal-plane field distribution is analyzed by a quadrant position detector (QPD) (New Focus 2911) at an acquisition rate of 20 kHz. A 532 nm bandpass filter in front of the QPD blocks beams with wavelengths different from the detection beam wavelength. The AOD permits control of the position of the beam focus. We also used it for the calibration procedures and for mapping the force distribution in the optical trap, as described in the text. A fluid chamber with microspheres was placed on a piezoelectric-controlled calibrated stage (Piezosystem Jena, Tritor 102) allowing three-dimensional translation. The inset shows an optically trapped sphere between the electrodes fed by noisy signals with controllable PSD.

The kinetic temperature of the optically trapped sphere is obtained from an analysis of the output signals of the position detection system. The system needs two calibration procedures: calibration of the position detection system and calibration of the force exerted by the trap on the sphere. At a given position of the quadrant position detector (QPD), the displacements of the sphere produce a unique and linear QPD response only within a restricted region of the probe displacement, usually several hundred nanometers. As we expect an increase of the amplitude of the displacements on application of an additional noise, the linearity range of the detection system and the force map of the optical trap should be characterized.

First, we calibrated the QPD measuring the ratio between the QPD output signals (in volts) and the real displacements of the probe (in nanometers) by using the natural thermal

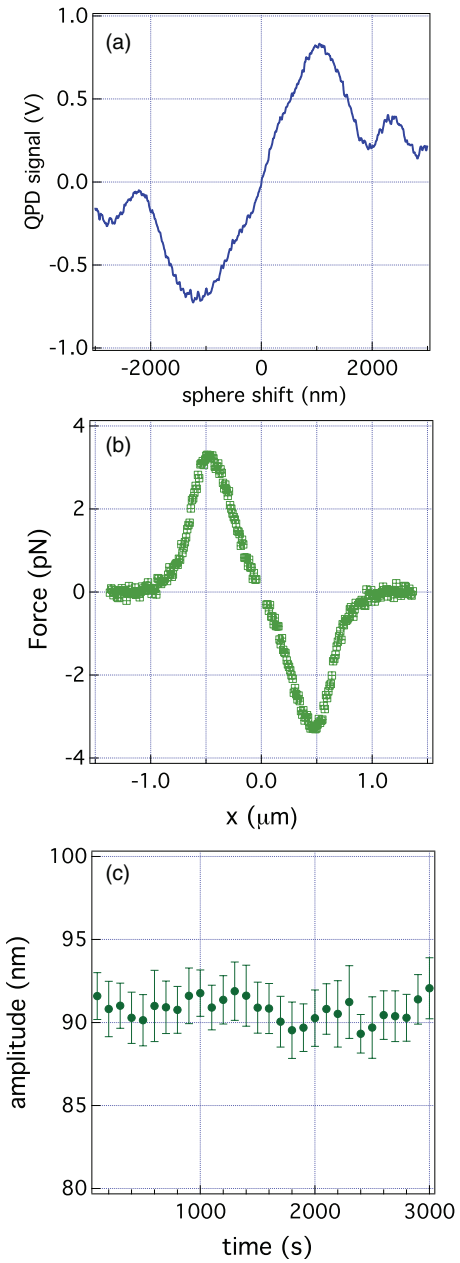

FIG. 2. (Color online) (a) The output signal of the QPD has a nonlinear character when the sphere displacements exceed ±1000 nm. The minor deviations from the linear dependence in the linear part of the QPD response are due to the nonuniformity in the detection beam intensity as well as the Brownian fluctuations of the sphere. (b) The force exerted on the 1 μm optically trapped sphere versus the radial distance from the trapping beam focus. The incident intensity of the trapping beam at the input pupil of the trapping objective is 5 mW. We confirmed that the force map is not affected by a further increase in the strong trap stiffness while maintaining the same intensity of the weak trap. (c) The amplitude of the sphere displacement in an ac electric voltage 30 V at 1 Hz over 3000 s.

fluctuations of the probe as described in [17]. The trap was calibrated in the absence of the additional force. Using a relatively strong trap where the Brownian fluctuations did not surpass several tens of nanometers, we first obtained the PSD of the position of the particle. The experimental PSD were then fitted to a Lorentzian function [17]

$$\mathrm{PSD}(f) = \frac{1}{2\pi^2\gamma}\,\frac{k_B T}{f^2 + f_c^2}, \tag{3}$$

where $f_c = \kappa/(2\pi\gamma)$ is the corner frequency. From the fit, we obtain the stiffness κ and the calibration coefficient $S_{\mathrm{QPD}}(\mathrm{nm/V})$ relating the QPD output signal with the absolute displacement of the sphere as described in [17]. In our experiment, $\kappa = 6$ pN/μm and $S_{\mathrm{QPD}} = 1280$ nm/V.

The spheres were trapped above the bottom surface of the fluid chamber at a distance of $\sim$20 μm controlled by the piezoelectric stage. The volume value of the viscous friction coefficient γ was corrected due to the proximity of the chamber surface using the Faxen law as described in [18].

Then we calibrated the acousto-optical deflector (AOD), measuring the ratio between the amplitude of the AOD input modulation signal V_{AOD} (in volts) and the corresponding sphere displacement (in nanometers) using the previously measured QPD calibration factor S_{QPD}. We moved the trapped sphere in the range of several tens of nanometers, changing the AOD modulation signal, and then measured the output signal of the QPD. This provided us with the calibration factor $S_{\mathrm{AOD}}(\mathrm{nm}/V_{\mathrm{AOD}})$ for the small range of the sphere displacement. We then confirmed with an image analysis that this factor holds for the AOD modulation amplitudes corresponding to the sphere displacements of ±3 μm.

Figure 2(a) shows the dependence of the QPD output signal on the shift of the sphere achieved by changing the AOD modulation voltage. The linear relationship between the displacements of the optically trapped sphere and the output signal of the position detection system can be seen within the range ±1000 nm. The linear range of the position detection can be extended further using a method suggested recently in [19].

Finally, we measured the map of the forces that the optical trap exerted on the sphere. These measurements define a range where the linear relationship between the optical force and the sphere displacement is valid. Within this range, the Langevin equation (1) can be used to define the effective kinetic temperature. The force map was characterized by the method proposed in [20]. In that method, a strong, stationary, and previously calibrated trap holds a sphere of a given diameter. The optical trapping potential of this trap is strong enough that external forces cannot move the sphere out of the range of the harmonic approximation. The intensity of the second trap, whose optical trapping potential for the given sphere has to be analyzed, is adjusted to be low. Its optical force acts as a perturbation exerted on the probe. When the second trap is scanning near the strong trap, it produces a variable force measured through the displacement of the probe in the strong trap.

To experimentally realize this technique, we used the AOD in a time-sharing regime [21]. The individual traps are not generated simultaneously, but a single optical beam is rapidly switched between a number of optical focuses by changing the frequency of the acoustic waves propagating in the AOD. Multiple optical traps are possible, as long as the focused beam is returned to the same location faster than the time it takes for the probe to diffuse away from that location, which is typically on the order of tens of milliseconds. That permits generating a dual trap with controllable distances between

the traps and a controllable ratio of their stiffnesses. The alternation of the trap positions is controlled by timing signals generated by a modulation generator adjusted to give a low frequency square wave with a controllable duty ratio. The analog voltage is transferred to the modulation input of a rf driver. The driver's rf output is then transferred to the AOD. The relative optical intensity in each trap depends on the duty ratio of the modulation signal, and the distance between the traps is determined by the period of the square wave. The calibration procedures described above permit expressing the experimental data in terms of the absolute values of the forces (pN) and the sphere displacements (nm).

Figure 2(b) illustrates the force map of the optical trap used in the experiments. The linear range of the restoring optical force extends up to ±500 nm. A slight deviation from linearity for small displacements from the center of the potential has been mentioned earlier, in [22].

To characterize the stability of the electric charges on a sphere, we applied a 1 Hz sinusoidal voltage to the electrodes of the electrophoretic chamber; this is within the frequency range of the white noise used in this study. One can also expect changes in the electrical conditions at low frequencies due to possible electrochemical reactions. The amplitude of the displacement of the optically trapped sphere measured with the position detection system did not change more than 6% over at least 3000 s (Fig. 2).

III. EXPERIMENTAL RESULTS

A. A Brownian sphere in a stationary trap with additional noise

We first analyzed the time traces of the position of the sphere in the optical trap with a given trap stiffness, both with and without the external force $\zeta(t)$. Figure 3 illustrates the PSDs of the position of the sphere, and Fig. 4 illustrates the histograms of the position of the sphere. As can be seen, the maximal sphere Brownian excursions without the additional noise do not exceed ±50 nm, however with the additional stochastic force the maximal amplitude may be ±250 nm. But even in this case, the sphere displacements do not exceed the linear ranges of either the position detection system or the harmonic approximation of the optical trapping potential. At a given value of the noisy voltage at the electrodes (∼200 V in our experiments), the maximal broadening of the position histogram strongly depends on the design of the electrophoretic chamber, since this design defines the value of the electric field near the optically trapped sphere. For the proof of principle experiments described in this paper, the absolute values of the charge of the sphere and the electric fields can change the results only quantitatively. What is important is that (1) the motion of the sphere in the sinusoidal field has a constant amplitude over one hour (see above), and (2) the broadening and compressing of the histograms of the position of the sphere are reversible when we switch on and off the noisy electric field.

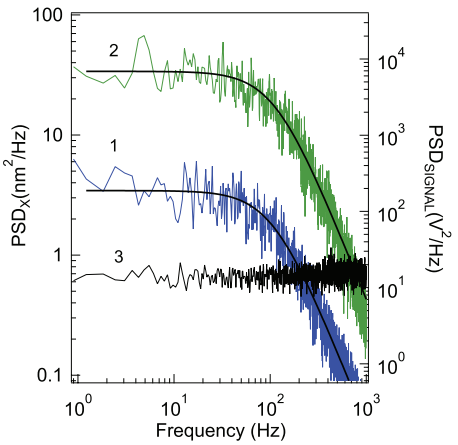

FIG. 3. (Color online) PSD of the position of the sphere without (blue curve, 1) and with (green curve, 2) the additional stochastic force. Solid black lines correspond to the Lorentzian fits. The power spectral density of the input noisy signal measured at the electrodes of the fluid cell is also shown (black line, 3). Both axes are in $\log_{10}$ scale.

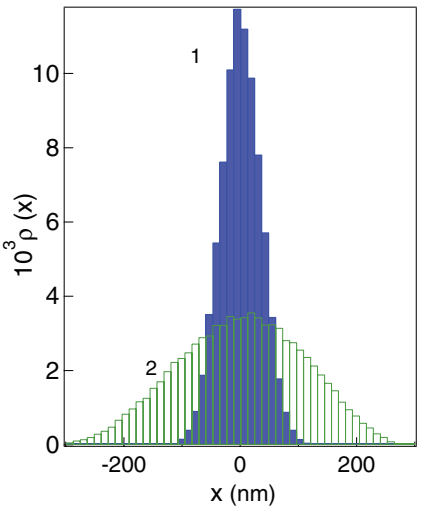

FIG. 4. (Color online) Histograms of the sphere position without (1) and with the additional stochastic force (2) corresponding to the PSD curves (1) and (2) shown in Fig. 3.

The parameters of the computer-controlled generator allowed us to obtain a constant spectrum of the electrical signal for frequencies up to 1 kHz. As can be seen in Fig. 3, the PSD in the presence of the additional force is also Lorentzian and, as expected, the corner frequency f_c does not change, since it is a function only of κ and γ. On the other hand, the whole PSD increases due to the external force, which can be interpreted as an increase of the effective kinetic temperature. This increase of temperature can also be observed in the stationary probability density $\rho(x)$ of the position of the sphere, depicted in Fig. 4. The additional force clearly broadens the histogram.

The following experiment demonstrates how fast one can switch the effective kinetic temperature of a Brownian particle. We studied the temporal response of the amplitude of the random motion of the particle to abrupt changes in the amplitude of the additional noise. Figure 5 shows that the position of the sphere (and hence the kinetic temperature) changes at the same rate as the electric field amplitude, so that only the relaxation time of the trap ($\tau_r = \gamma/\kappa = 1.4$ ms in our experimental conditions) is the limiting factor.

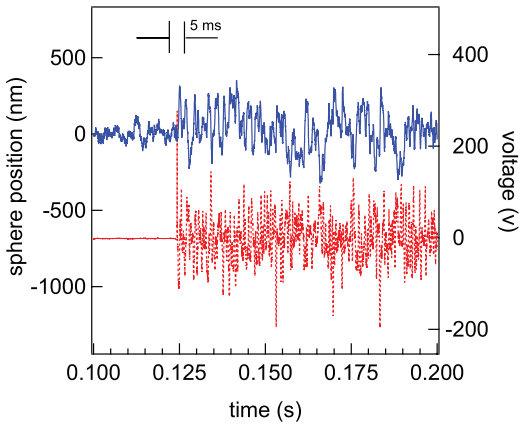

FIG. 5. (Color online) The sphere position (blue solid curve, left axis) and amplitude of electric signal (red dot curve, right axis) as a function of time if the electric field changes abruptly.

B. Kramers transitions in the presence of additional white noise

We now consider the motion of the sphere in the presence of the additional stochastic force in an optical trap with a more complex structure, namely, that of a double-well optical potential. As is well known, Kramers transitions [23]—thermally activated escape over a potential barrier—may occur in this case. Kramers transitions are important factors in many chemical, physical, and biological phenomena. To realize Kramers transitions, the optical traps of the dual-well trapping potential have to be close to each other, and the thermal energy has to be large enough to drive the sphere over the potential barrier between neighboring optical traps. The probability distribution of residence times, i.e., of the intervals of time between escape events from trap to trap (the Kramers transition rate) in the overdamping regime depends on the height of the potential barrier and the absolute temperature of the system [23]. Experimental results [24] at room temperature are well described by the Kramers theory.

In our experiments, we showed that the additional noise decreased the residence time corresponding to a new center of mass temperature. We created a double-well potential with a controllable distance between the two traps and controllable trap depths using a time-sharing protocol for the AOD. Figure 6(a) shows a fragment of the time traces of the 1 μm diameter sphere moving in the double-well potential when at a given moment of time the additional noise signal was switched on. The spatial probability density of the sphere $\rho(x)$ is related to the potential energy profile of the trap $U(x)$ as $\rho(x) = Z^{-1}\exp[U(x)/k_BT]$, where Z is the partition function. We measured the probability density of the position without additional noise from a time series $x(t)$, and the potential $U(x)$ was found with two wells separated by a barrier whose energy is above the thermal energy k_BT, as shown in Fig. 6(b). Figure 6(c) shows the residence time probability distribution without and with the additional noise signals. As predicted by Kramers [23], the residence time probability decays exponentially with the residence time. Notice that in the presence of the additional noise, the probability distribution decays faster, which is consistent with an increase of the effective temperature.

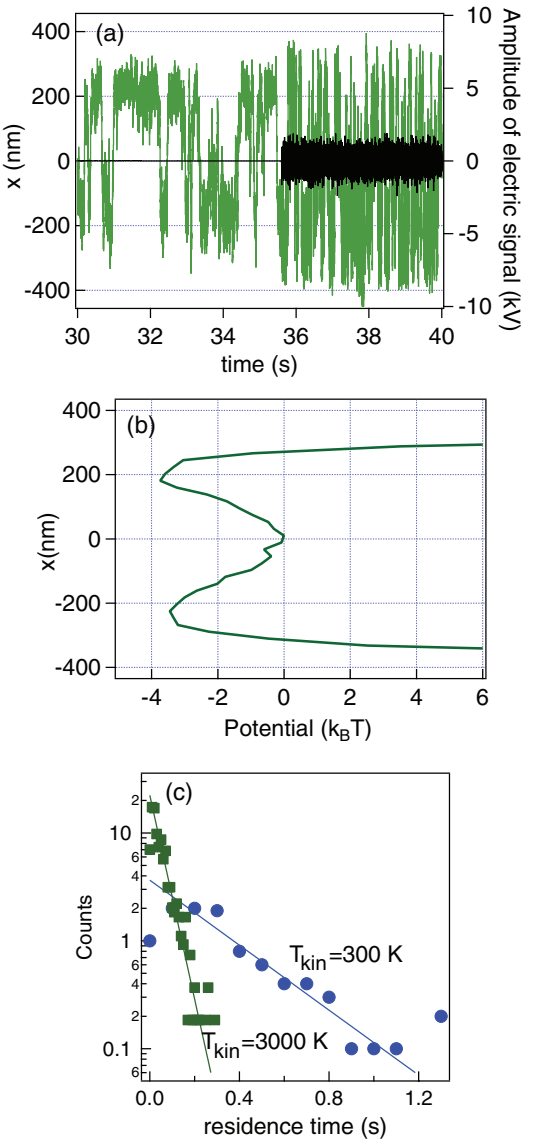

FIG. 6. (Color online) (a) The position traces (green lines, left axis) of the sphere in the double-well potential. The black lines (right axis) show the voltage on the electrodes. The additional noisy signal was switched on at 35.5 s. As can be seen, the frequency of the Kramers transitions increases. (b) The trapping potential obtained at room temperature. (c) Probability of the residence time of the Kramers transitions (in counts, $\log_{10}$ scale) at room temperature (green squares) and at 3000 K (blue circles).

C. A nonequilibrium process

For a complete characterization of the effective thermal bath, we studied the dynamics of the particle in a nonequilibrium situation. The response of the Brownian particle to an external driving force is related to the temperature. The fluctuation-dissipation relation is a mathematical identity relating the temperature, the response close to equilibrium, and the time correlations of the unperturbed system. The Crooks fluctuation theorem (CFT) [25] goes further, establishing a relationship between the probability density function (PDF) of the work W along a process arbitrarily far from equilibrium, $\rho(W)$, and the PDF of the work in the time-reversed process,

$\rho^*(W)$. Notice that the CFT goes beyond the fluctuation-dissipation relationship and is valid not only in the linear but also in the nonlinear response limit.

Suppose the system starts at equilibrium states at temperature T both in the forward and time-reversed processes. If the free energy difference between the final and initial states (of the forward process) is $\Delta F = F_{\rm fin} - F_{\rm ini}$, the Crooks theorem states that

$$\ln\left[\frac{\rho(W)}{\rho^*(-W)}\right] = \frac{W - \Delta F}{k_B T}, \tag{4}$$

and this has been checked both in simulations and experiments for processes at room temperature [26–28].

We implemented the nonequilibrium protocol depicted in Fig. 7. In the first step, the trap center is moved from $x_0 = -L$ to $x_0 = +L$ at constant velocity $v = 2L/\tau$, where $L = 61$ nm and $\tau = 6.3$ ms. This is the forward process. We then let the sphere relax to the new equilibrium position, keeping the trap center at $x_0 = +L$ for the same time $\tau = 6.3$ ms, which is larger than the relaxation time of the trap, $\tau_r = \gamma/\kappa = 1.4$ ms. Then the trap is moved back from $x_0 = +L$ to $x_0 = -L$ with the same velocity $-v$ (reverse process) and it is held fixed at $x_0 = -L$ for the same time τ. This protocol was repeated $\sim 10^4$ times. During the protocol, the position of the sphere was monitored, and the position traces are shown in Fig. 7. In each cycle we calculated the work in the forward and time-reversed processes following [29], where the work done by an external agent in a microscopic system during an arbitrarily far from equilibrium process is introduced. If the nonequilibrium driving is described by the evolution of a control parameter $\lambda(t)$, the work done along the process is given by

$$W = \int_{\lambda(0)}^{\lambda(\tau)} \frac{\partial V(x(t),\lambda(t))}{\partial \lambda} \circ d\lambda(t), \tag{5}$$

where $\circ$ means that the integral is taken in the Stratonovich sense, and V is the trapping potential. In our case, the control parameter is the position of the trap center, $\lambda(t) = x_0(t)$. Notice

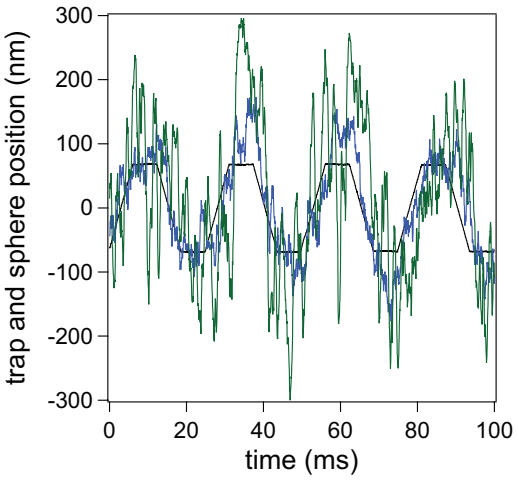

FIG. 7. (Color online) The position of the center of the trap (black line) and the positions of the sphere as functions of time without external electric field (blue curve) and with noisy electric field (green curve).

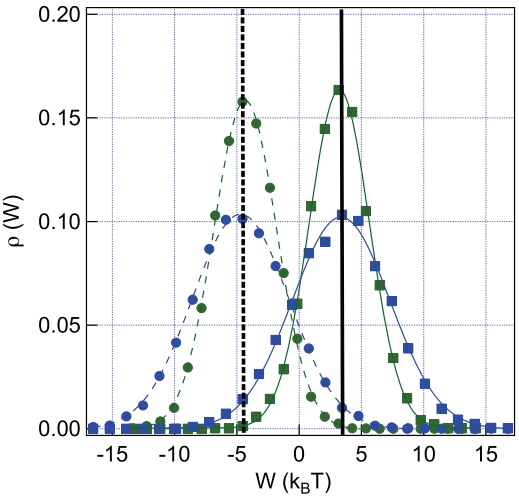

FIG. 8. (Color online) The probability density function of the work obtained in around 7000 realizations of the forward process $[\rho(W)]$, and the probability density function obtained from the same number of realizations of the reverse process $[\rho^*(-W)]$. The vertical black lines represent the analytical value of the average work in the forward process calculated using (13) (solid line) and the average of $-W$ in the reverse process (dashed line) which is calculated in a way analogous to (13). The squares correspond to the forward process $[\rho(W)]$ and the circles to the reverse $[\rho^*(-W)]$. The solid and dashed curves are Gaussian fits.

that the work is a stochastic quantity that depends on the trajectory followed by the particle, $x(t)$.

Figure 8 shows the experimental values of the probability density of the work $\rho(W)$ $[\rho^*(-W)]$ in the forward (reverse) process. We found that they have Gaussian distributions intersecting approximately at $W = 0$ since in our case $\Delta F = 0$.

IV. DISCUSSION

We consider first the experimental results on the motion of the sphere in a stationary trap with additional noise (Figs. 3 and 4). As we have seen, the kinetic temperature affects both the autocorrelation and the equilibrium histogram of the position of the bead. Consequently, we can define two kinetic temperatures, either from the data for the PSD or using $\rho_{\rm ss}(x)$. As we show below, these two kinetic temperatures can differ if the additional noise is not white.

From the Langevin equation (1), we calculate (see the details in Appendix A) both the PSD and the stationary probability distribution $\rho_{\rm ss}(x)$ for an external noise $\zeta(t)$ with arbitrary correlation $\langle \zeta(t)\zeta(t')\rangle = \sigma^2 \Gamma(t - t')$, with $\int_{-\infty}^{\infty} \Gamma(t)dt = 1$. The PSD is

$$\mathrm{PSD}(f) = \frac{1}{4\pi^2\gamma^2} \frac{2\gamma k_B T + \sigma^2 \tilde{\Gamma}(f)}{f^2 + f_c^2}, \tag{6}$$

where $\sigma^2\tilde{\Gamma}(f)$ is the Fourier transform of the correlation function of the external noise. If $\tilde{\Gamma}(f)$ is constant for frequencies much higher than the corner frequency of the trap f_c, then the PSD (6) is approximately a Lorentzian function with the same corner frequency. We can define the following

effective kinetic temperature, which we denote by $T_{\rm PSD}$:

$$T_{\rm PSD} \equiv \frac{2\pi^2 \gamma f_c^2\, {\rm PSD}(0)}{k_B} = T + \frac{\sigma^2}{2k_B\gamma}. \tag{7}$$

Notice that, with this definition, $T_{\rm PSD}$ does not depend on the shape of the correlation function of the noise, $\Gamma(t)$.

On the other hand, we can define the following kinetic temperature derived from the histogram:

$$T_{\rm hist} \equiv \frac{\kappa \langle x^2 \rangle_{\rm ss}}{k_B}. \tag{8}$$

The stationary probability density $\rho_{\rm ss}(x)$ can also be calculated (see Appendix A) and it is Gaussian with zero mean and dispersion

$$\langle x^2 \rangle_{\rm ss} = \frac{k_B T}{\kappa} + \frac{\sigma^2}{\gamma\kappa}\int_0^\infty dt\, e^{-\kappa t/\gamma}\, \Gamma(t), \tag{9}$$

yielding

$$T_{\rm hist} = T + \frac{\sigma^2}{\gamma k_B}\int_0^\infty dt'\, \Gamma(t') e^{-t'/\tau_r}, \tag{10}$$

$\tau_r = \gamma/\kappa$ being the relaxation time of the particle in the trap. If $\Gamma(t)$ is peaked around $t = 0$ and the correlation time of the noise, given by $\tau_c \equiv \int_0^\infty dt\, t\Gamma(t)$, is small compared to τ_r, $T_{\rm hist}$ is approximately

$$T_{\rm hist} \simeq T + \frac{\sigma^2}{2k_B\gamma}\left(1 - \frac{2\tau_c}{\tau_r}\right). \tag{11}$$

Notice that $T_{\rm hist}$, unlike $T_{\rm PSD}$ as defined by (7), does depend on the correlation time of the noise. The difference between $T_{\rm PSD}$ and $T_{\rm hist}$ is proportional to τ_c/τ_r, therefore it vanishes if the external noise is white. In our experiments, $\tau_r = 1.4$ ms and $\tau_c = 0.26$ ms, with τ_c obtained experimentally from the spectral analysis of the voltage at the electrodes (see below).

In our setup, we achieved a constant spectrum of the noise only up to 1 kHz (Fig. 3). We measured the autocorrelation function of the signal on the electrodes $V(t)$, defined in [30] $\tilde{\Gamma}(t) = \frac{\langle V(t')V(t'+t)\rangle}{\langle V(t')V(t')\rangle}$, which can be fitted to the function $\tilde{\Gamma}(t) = \exp[-(t/\tau_c)^2]\cos(\frac{t}{\tau_o})$, with $\tau_c = 0.26$ ms and $\tau_o = 0.17$ ms. The correlation of the noise is related to $\tilde{\Gamma}(t)$ by $\Gamma(t) = N\tilde{\Gamma}(t)$, where N is a normalization constant such that $\int_{-\infty}^{\infty}\Gamma(t)dt = N\int_{-\infty}^{\infty}\hat{\Gamma}(t)dt = 1$. The full expression of the correlation function of the additional noise is

$$\Gamma(t) = \frac{e^{t c^2/4t_o^2}}{\sqrt{\pi}}\frac{e^{-(t/\tau_c)^2}}{\tau_c}\cos(t/t_o). \tag{12}$$

Figure 10 presents a quantitative summary of our measurements performed with different intensities of the additional noise signal. We increased the intensity of the noisy voltage and from (7) we found $\sigma^2/(2k_B\gamma)$, which is a measure of the noise intensity in kelvin. We plot the effective temperatures $T_{\rm PSD}$ and $T_{\rm hist}$ as functions of $T_e = \sigma^2/(2k_B\gamma)$. We observed experimentally that $T_{\rm hist}$ and $T_{\rm PSD}$ coincide within statistical errors.

We now consider the experimental results on the out of equilibrium process (Figs. 7–9). As seen in Fig. 8, the experimental value of the average work is close to the analytical value of the average of the work done over a time τ over the ensemble of trajectories [31], which for the forward process is obtained by integrating the Langevin equation (1) (see Appendix B for details):

$$\langle W \rangle = \gamma v^2 \tau\left[1 + \frac{\tau_r}{\tau}(e^{-\tau/\tau_r} - 1)\right]. \tag{13}$$

This result is not affected by the addition of the external noise because the work depends linearly on the additional noise, whose average is zero. Notice also that for slow driving ($\tau/\tau_r \gg 1$) we recover the Stoke's limit $\langle W \rangle \simeq \gamma v^2 \tau$. The analytical value of the work in the forward process without an external field is $\langle W \rangle = 14.34$ pN nm, whereas the experimental value is $W_{\rm exp} = (15.06 \pm 0.14)$ pN nm. Note that we underestimated the actual error of the work since we only took into account the statistical dispersion of the data but not the experimental error. An error of 0.1 pN in the force and 1 nm in the position would yield approximately an additional error which might be of the same order of magnitude as the statistical error. We also show in Fig. 8 that the PDFs of the work get wider when we increase the amplitude of the external noise, as expected.

We introduce a new effective temperature, the *Crooks temperature* T_C, to check the consistency of our effective thermal bath for nonequilibrium processes. We define T_C by the inverse of the slope (divided by k_B) of the linear fit to $\ln[\frac{\rho(W)}{\rho^*(-W)}]$ as a function of W, following (4). The work distributions are Gaussian and in this case Crooks's theorem is given by a simple relationship between the average and the variance of the work,

$$T_C = \frac{\sigma_W^2}{2k_B\langle W \rangle}. \tag{14}$$

The expression for σ_W^2 is cumbersome and very sensitive to the specific form of the correlation of the external noise $\Gamma(t)$. T_C can be obtained analytically using (14) for a particle described by the Langevin equation (1) under an arbitrary external noise with correlation $\Gamma(t)$ and intensity σ^2, as shown in Appendix C. Depending on the shape of $\Gamma(t)$, we can get T_C larger or smaller than $T_{\rm hist}$, for example. The full expression of T_C in terms of the correlation of the additional noise and all the physical parameters of our system can be found in Appendix C.

Figure 9 shows that $\ln[\rho(W)/\rho^*(-W)]$ depends linearly on W with and without additional noise. We first test the validity of Crooks' theorem in the absence of external noise, where $\sigma^2 = 0$ and it is expected that $T_C = T$. The experimental effective temperatures are in this case $T_{\rm hist} = (310 \pm 3)$ K, $T_{\rm PSD} = (297 \pm 7)$ K, and $T_C = (283 \pm 1)$ K, the errors being purely statistical and therefore a lower bound on the real error. With external noise, the slope of $\ln[\rho(W)/\rho^*(-W)]$ as a function of W decreases when the amplitude of the external noise increases, indicating an increase of the effective Crooks temperature T_C.

We now try to explain, in terms of the finite correlation time of the noise, the deviation between T_C (Fig. 10) and the temperatures calculated from the position traces. We model the motion of the particle by the Langevin equation (1) with the noise correlation that fits the experimental data, given by (12). For $\Gamma(t)$ defined by (12), we obtain, using (10), $T_{\rm hist} = T + 0.95T_e$ which is slightly smaller than $T_{\rm PSD} = T + T_e$ (7)

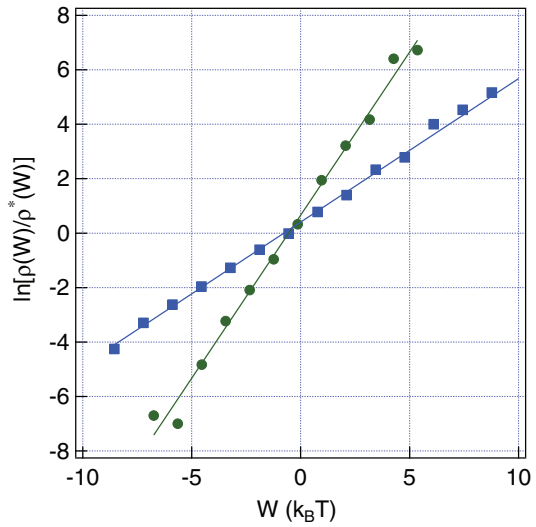

FIG. 9. (Color online) $\ln[\rho(W)/\rho^*(-W)]$ as a function of W/k_BT without (blue squares) and with additional noise (green circles) corresponding respectively to the PSD curves (1) and (2) shown in Fig. 3. The solid lines are linear fits to the experimental data.

and fits the experimental data. However, the analytical value of T_C for different noise intensities (the dashed line in Fig. 10), given by (14) is significantly above the experimental value of T_C. We notice that our calculations predict that both for slow

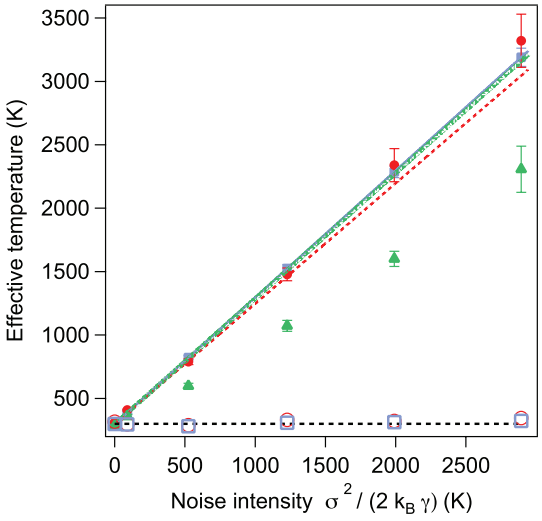

FIG. 10. (Color online) Effective kinetic temperatures as functions of $T_e = \sigma^2/(2k_B\gamma)$. The filled symbols correspond to experimental values of the effective temperature measured from the fluctuations and the response of the bead along the x axis (direction of the additional noise): $T_{\rm PSD}$ (blue filled squares), $T_{\rm hist}$ (red filled circles), and T_C (green filled triangles). Statistical errors are plotted in the error bars. Lines represent the analytical values obtained for nonwhite external noise $\zeta(t)$ with correlation function given by (12) for $T_{\rm PSD}$ (7) (blue solid line), $T_{\rm hist}$ (8) (red dashed line), and T_C (green dotted line), which was obtained analytically using (14). We also show, in open symbols, the experimental values of the effective temperature measured from the fluctuations along the y axis: $T_{\rm PSD}$ (blue open squares) and $T_{\rm hist}$ (red open circles). The statistical errors are smaller than the size of the symbols. The black dashed line is set to 300 K.

driving ($t/\tau_r \gg 1$) and in the white noise limit ($\tau_c/\tau_r \to 0$) all the temperatures collapse to a single line of slope unity: $T_{\rm PSD} = T_{\rm hist} = T_C = T + T_e$. Neither limit could be reproduced with our experimental setup because in moving the trap slower, the relative error of the work increases and the generator of our setup does not allow reducing τ_c.

The Langevin equation is valid for our system since the PSD of the position is Lorentzian. Therefore we can discard the supposition that the deviation between T_C and both $T_{\rm hist}$ and $T_{\rm PSD}$ observed in our experiment could be due to the finite bandwidth of the additional noise. We also measured the effective temperature from the traces along the y axis, that is, the axis that is orthogonal to the direction of the applied field. To do this, we had previously calibrated the trap in the y axis in the absence of external noise, where we found $\kappa_y = 5.5$ pN/μm and $S_{{\rm QPD},y} = 1700$ nm/V. When increasing the noise intensity, the effective temperature along the y axis remains constant and equal to the room temperature (see Fig. 10). Therefore, the difference between the experimental and the analytical values of T_C is not because of the presence of an extra degree of freedom where energy is being stored. The presence of torque can also be discarded, using the technique described in [32] (results not shown). Electrophoretic effects may explain this deviation: In our system, the particle feels a random force which is not exactly the signal recorded from the electrodes due to the reordering of the electric charges of the water molecules around the bead. This effect is enhanced when the trap is driven out of equilibrium. Notice that this constitutes a difference from the experiment in [13] where the trap center is moved randomly and the Crooks temperature tends to the equilibrium temperature when the correlation time of the external noise tends to zero.

In conclusion, we have presented an experimental technique that allows one to control the kinetic temperature of a Brownian particle over a wide range of values, from room temperature to several thousand kelvin. The environment created by the noisy external force mimics a high temperature reservoir within the limitations analyzed in this paper. Our technique opens the possibility of implementing a variety of nonisothermal processes. For example, the increase of temperature affects only one spatial direction. By coupling the coordinate of the particle along this direction with an orthogonal coordinate, one can effectively couple two thermal baths at different temperatures through a Brownian degree of freedom, as in the Feynman ratchet and other Brownian motors and refrigerators. One could also implement adiabatic processes by designing a protocol where $\rho(x)$, and therefore the entropy of the system along a stochastic trajectory [33], $S(t) = -k_B \ln \rho(x,t)$, does not change in time. The density $\rho(x)$ can be kept constant in time with our setup by changing the stiffness of the trap and the intensity of the external random force in a synchronous way.

ACKNOWLEDGMENTS

I.M. and D.P. acknowledge financial support from the Fundació Privada Cellex Barcelona, Generalitat de Catalunya Grant No. 2009-SGR-159, and from the Spanish Ministry of Science and Innovation (MICINN FIS2008-00114, FIS2011-24409). E.R. and J.M.R.P. acknowledge fruitful discussions with Jordan M. Horowitz and Luis Dinís, and financial support

from grants MOSAICO, ENFASIS (the Government of Spain), and MODELICO (the Comunidad de Madrid).

APPENDIX A: CALCULATION OF $T_{\rm hist}$

We consider a Brownian particle whose motion is described by the Langevin equation (1),

$$\gamma\dot{x}(t) = -\kappa x(t) + \xi(t) + \zeta(t), \tag{A1}$$

where $\xi(t)$ and $\zeta(t)$ are Gaussian noises with zero average $\langle\xi(t)\rangle = \langle\zeta(t)\rangle = 0$ and correlation functions

$$\langle\xi(t)\xi(t')\rangle = 2k_BT\gamma\delta(t-t'), \tag{A2}$$

$$\langle\zeta(t)\zeta(t')\rangle = \sigma^2\Gamma(t-t'). \tag{A3}$$

The solution of (A1) is

$$x(t) = x(0)e^{-t/\tau_r} + \frac{e^{-t/\tau_r}}{\gamma}\int_0^t ds\, e^{s/\tau_r}[\xi(s)+\zeta(s)], \tag{A4}$$

where $\tau_r = \gamma/\kappa$ is the relaxation time in the trap. If we multiply $x(t)$ by (A1), and we take the average over all trajectories, we get

$$\frac{\gamma}{2}\frac{d\langle x^2\rangle}{dt} = -\kappa\langle x^2\rangle + \langle\xi x\rangle + \langle\zeta x\rangle, \tag{A5}$$

where $\langle\xi x\rangle$ and $\langle\zeta x\rangle$ can be calculated using Novikov's theorem [34–36]:

$$\langle\zeta(t)x(t)\rangle = \int_0^t ds\langle\zeta(t)\zeta(s)\rangle\left\langle\frac{\delta x(t)}{\delta\zeta(s)}\right\rangle. \tag{A6}$$

Using (A4), $\langle\frac{\delta x(t)}{\delta\zeta(s)}\rangle = \frac{1}{\gamma}e^{-(t-s)/\tau_r}$, and therefore

$$\langle\zeta(t)x(t)\rangle = \frac{\sigma^2}{\gamma}\int_0^t ds\,\Gamma(t-s)e^{-(t-s)/\tau_r}, \tag{A7}$$

whereas for the thermal noise,

$$\langle\xi(t)x(t)\rangle = \int_0^t ds\langle\xi(t)\xi(s)\rangle\left\langle\frac{\delta x}{\delta\xi(s)}\right\rangle = k_BT. \tag{A8}$$

Using (A7) and (A8), we can rewrite (A5) as

$$\frac{\gamma}{2}\frac{d\langle x^2\rangle}{dt} = -\kappa\langle x^2\rangle + k_BT + \frac{\sigma^2}{\gamma}\int_0^t dt'\,\Gamma(t')e^{-t'/\tau_r}. \tag{A9}$$

In the steady state, $t\to\infty$ and $d\langle x^2\rangle/dt = 0$. In this limit, the above equation yields (9):

$$\kappa\langle x^2\rangle_{\rm ss} = k_BT + \frac{\sigma^2}{\gamma}\int_0^\infty dt'\,\Gamma(t')e^{-t'/\tau_r}. \tag{A10}$$

By using the equipartition theorem, we get $T_{\rm hist}$ as a function of the mean square displacement in the steady state,

$$T_{\rm hist} = \frac{\kappa\langle x^2\rangle_{\rm ss}}{k_B} = T + \frac{\sigma^2}{\gamma k_B}\int_0^\infty dt'\,\Gamma(t')e^{-t'/\tau_r}, \tag{A11}$$

which proves (8).

We notice that $\Gamma(t)$ has a characteristic time scale given by τ_c, so it can be expressed as a function of t/τ_c, say $\Gamma(t) = \Gamma(t/\tau_c)$. The correlation of the noise decays in this time scale, which means that the integral in the above equation can be expressed, by using the change of variable $s = t/\tau_r$, by

$$\int_0^\infty dt'\,\Gamma(t'/\tau_c)e^{-t'/\tau_r} = \tau_r\int_0^\infty ds\,\Gamma\left(\frac{\tau_r}{\tau_c}s\right)e^{-s}. \tag{A12}$$

If $\tau_c \ll \tau_r$, the exponential decays much more slowly in s than does the correlation of the noise in the units above, therefore it can be approximated by $e^{-s}\simeq 1-s$:

$$\int_0^\infty dt'\Gamma(t'/\tau_c)e^{-t'/\tau_r} \simeq \tau_r\int_0^\infty ds\Gamma\left(\frac{\tau_r}{\tau_c}s\right)(1-s) = \frac{1}{2} - \frac{\tau_c}{\tau_r}. \tag{A13}$$

For the last equality, we have used that $\Gamma(t)$ is normalized, $\int_{-\infty}^\infty dt\,\Gamma(t/\tau_c) = 1$, that it is symmetric around $t = 0$, and the definition of the correlation time of the noise $\tau_c = \int_0^\infty dt, t\Gamma(t/\tau_c)$. By substituting (A13) into (A11), we prove (11):

$$T_{\rm hist} \simeq \frac{\sigma^2}{2\gamma k_B}\left(1 - \frac{2\tau_c}{\tau_r}\right). \tag{A14}$$

APPENDIX B: CALCULATION OF $\langle W\rangle$

We now calculate the average of the work done when moving the trap center at a constant velocity v for a period of time t. In this situation, the work done to move a trap that creates a moving quadratic potential $V(x(t),x_0(t)) = \frac{\kappa}{2}[x - x_0(t)]^2$ is equal to

$$W = \int_0^t -\kappa(x - vt')v\,dt' = -\kappa v\int_0^t y(t')dt', \tag{B1}$$

where we have used the definition of work in (5), used $x_0(t) = vt$ as a control parameter, and introduced the variable $y(t) = x(t) - vt$. Here, $y(t)$ satisfies the following Langevin equation:

$$\gamma\dot{y}(t) = -\kappa y(t) - \gamma v + \xi(t) + \zeta(t), \tag{B2}$$

whose solution is

$$y(t) = y(0)e^{-t/\tau_r} + \frac{e^{-t/\tau_r}}{\gamma}\int_0^t ds\, e^{s/\tau_r}[-\gamma v + \xi(s) + \zeta(s)]. \tag{B3}$$

The average over trajectories is

$$\langle y(t)\rangle = \langle y(0)\rangle e^{-t/\tau_r} - v\tau_r[1 - e^{-t/\tau_r}] = -v\tau_r[1 - e^{-t/\tau_r}], \tag{B4}$$

where $\langle y(0)\rangle = \langle x(0)\rangle = 0$, since the bead is initially in equilibrium oscillating around the trap center located in $x = 0$. The average work is

$$\langle W\rangle = -\kappa v\int_0^t\langle y(t')\rangle dt' = \gamma v^2 t + \frac{\gamma^2v^2}{\kappa}[e^{-t/\tau_r} - 1], \tag{B5}$$

which is the expression that we introduced in (13).

APPENDIX C: CALCULATION OF T_C

For a process in which a physical system that starts in equilibrium and then is driven out of equilibrium in such a way that the probability distribution of the work is Gaussian, the Crooks temperature is equal to (14):

$$T_C = \frac{\sigma_W^2}{2k_B\langle W\rangle}, \tag{C1}$$

where $\langle W\rangle$ is given by (13). We are now interested in calculating the variance of the work done in the nonequilibrium process consisting of moving the trap at a constant velocity v over a time t, which we denote by σ_W^2. We first notice that the work is defined in terms of the variable $y(t) = x(t) - vt$ by (B1). If we introduce the random variables

$$\begin{aligned} q_\xi(t') &= \int_0^{t'} ds\, e^{-(t'-s)/\tau_r}\xi(s), \\ q_\zeta(t') &= \int_0^{t'} ds\, e^{-(t'-s)/\tau_r}\zeta(s), \end{aligned} \tag{C2}$$

then $y(t)$ can be rewritten as

$$y(t) = y(0)e^{-t/\tau_r} - v\tau_r[1 - e^{-t/\tau_r}] + \frac{1}{\gamma}[q_\xi(t) + q_\eta(t)]. \tag{C3}$$

By substituting this formula in (B1), we get

$$\begin{aligned} W = &-\gamma v y(0)[1 - e^{-t/\tau_r}] \\ &+\langle W\rangle - \frac{\kappa v}{\gamma}\int_0^t dt'[q_\xi(t') + q_\zeta(t')]. \end{aligned} \tag{C4}$$

Therefore, the work is a linear combination of independent random variables. This implies that the variance of the work is

$$\sigma_W^2 = \gamma^2 v^2[1 - e^{-t/\tau_r}]^2\sigma_{x(0)}^2 + \frac{\kappa^2 v^2}{\gamma^2}\sigma_{q_\xi}^2 + \frac{\kappa^2 v^2}{\gamma^2}\sigma_{q_\zeta}^2. \tag{C5}$$

The first term involves the variance of the position at $t = 0$ in equilibrium, $\sigma_{x(0)}^2$, which is known [see (A11)], and so

$$\sigma_{x(0)}^2 = \frac{k_B T_{\rm hist}}{\kappa}. \tag{C6}$$

The calculation of $\sigma_{q_\xi}^2$ and $\sigma_{q_\zeta}^2$ is not straightforward. The first can be calculated analytically, whereas the second can be calculated only when the correlation function of the external noise takes on particular forms. We now show how a closed expression for the term involving the thermal noise, $\sigma_{q_\xi}^2$, can be derived. This variance is defined by

$$\sigma_{q\xi}^2 = \int_0^t dt_1 \int_0^t dt_2 \langle q_\xi(t_1)q_\xi(t_2)\rangle, \tag{C7}$$

where

$$\begin{aligned} \langle q_\xi(t_1)q_\xi(t_2)\rangle = \sigma^2 \int_0^{t_1} dt' \int_0^{t_2} dt''\, e^{-(t_1-t')/\tau_r} e^{-(t_2-t'')/\tau_r}\Gamma \\ \times (t' - t''). \end{aligned} \tag{C8}$$

For thermal Gaussian white noise, $\sigma^2 = 2\gamma k_B T$ and $\Gamma(t' - t'') = \delta(t' - t'')$, which implies

$$\langle q_\xi(t_1)q_\xi(t_2)\rangle = k_B T\frac{\gamma^2}{\kappa}[e^{-|t_1-t_2|/\tau_r} - e^{-(t_1+t_2)/\tau_r}]. \tag{C9}$$

By substituting this into (C7), and integrating, we obtain

$$\sigma_{q\xi}^2 = 2k_B T\frac{\gamma^3}{\kappa^2}t + k_B T\frac{\gamma^4}{\kappa^3}[4e^{-t/\tau_r} - e^{-2t/\tau_r} - 3]. \tag{C10}$$

After some algebra, T_C can be expressed as a function of $T_e = \sigma^2/2k_B\gamma$ for any correlation function $\Gamma(t)$:

$$T_C = T + \frac{\mathcal{L}\{\Gamma(t)\}(1/\tau_r) + \frac{1}{\tau_r^3}\int_0^t dt_1 \int_0^t dt_2 \int_0^{t_1} dt' \int_0^{t_2} dt''\, e^{-(t_1-t')/\tau_r} e^{-(t_2-t'')/\tau_r}\Gamma(t' - t'')}{\frac{t}{\tau_r} + e^{-t/\tau_r} - 1}\, T_e, \tag{C11}$$

where $\mathcal{L}\{\Gamma(t)\}(1/\tau_r)$ is the Laplace transform of $\Gamma(t)$ evaluated at $s = 1/\tau_r$,

$$\mathcal{L}\{\Gamma(t)\}(1/\tau_r) \equiv \int_0^\infty dt'\, \Gamma(t')e^{-t'/\tau_r}. \tag{C12}$$

For the correlation function (12) that fits the experimental data, (C11) can only be calculated numerically. In the limit in which the external noise is white, i.e., $\sigma^2 = 2\gamma k_B T_e$ and $\Gamma(t) = \delta(t)$, we obtain a result analogous to (C10) but replacing T by T_e. Only in this case is $T_C = T_{\rm hist} = T_{\rm PSD} = T + T_e$ for any value of the driving time τ.

[1] A. Ashkin and J. Dziedzic, Appl. Phys. Lett. **30**, 202 (1977).
[2] T. Li, S. Kheifets, and M. G. Raizen, Nat. Phys. **7**, 527 (2011).
[3] J. Gieseler, B. Deutsch, R. Quidant, and L. Novotny, Phys. Rev. Lett. **109**, 103603 (2012).
[4] C. Bustamante, J. Liphardt, and F. Ritort, Phys. Today **58**(7), 43 (2005).
[5] S. Ciliberto, S. Joubaud, and A. Petrosyan, J. Stat. Mech. (2010) P12003.
[6] A. Bérut, A. Arakelyan, A. Petrosyan, S. Ciliberto, R. Dillenschneider, and E. Lutz, Nature (London) **483**, 187 (2012).
[7] L. I. McCann, M. Dykman, and B. Golding, Nature (London) **402**, 785 (1999).
[8] V. Blickle and C. Bechinger, Nat. Phys. **8**, 143 (2011).
[9] R. Radunz, D. Rings, K. Kroy, and F. Cichos, J. Phys. Chem. A **113**, 1674 (2009).

[10] P. V. Ruijgrok, N. R. Verhart, P. Zijlstra, A. L. Tchebotareva, and M. Orrit, Phys. Rev. Lett. **107**, 037401 (2011).
[11] H. Mao, J. R. Arias-Gonzalez, S. B. Smith, I. Tinoco, and C. Bustamante, Biophys. J. **89**, 1308 (2005).
[12] C. Gosse and V. Croquette, Biophys. J. **82**, 3314 (2002).
[13] J. R. Gomez-Solano, L. Bellon, A. Petrosyan, and S. Ciliberto, Europhys. Lett. **89**, 60003 (2010).
[14] F. Beunis, F. Strubbe, K. Neyts, and D. Petrov, Phys. Rev. Lett. **108**, 016101 (2012).
[15] P. Mestres and D. Petrov, Eur. Biophys. J. **40**, 1081 (2012).
[16] G. Volpe, S. Perrone, J. M. Rubi, and D. Petrov, Phys. Rev. E **77**, 051107 (2008).
[17] K. Visscher, S. P. Gross, and S. M. Block, IEEE J. Sel. Top. Quantum Electron. **2**, 1066 (1996).
[18] K. Svoboda and S. M. Block, Annu. Rev. Biophys. Biomol. Struct. **23**, 247 (1994).
[19] I. A. Martinez and D. Petrov, Appl. Opt. **51**, 5973 (2012).
[20] A. A. R. Neves, A. Fontes, L. de Y. Pozzo, A. A. de Thomaz, E. Chillce, E. Rodrigez, L. C. Barbosa, and C. L. Cesar, Opt. Express **14**, 13101 (2006).
[21] I. A. Martinez and D. Petrov, Appl. Opt. **51**, 5522 (2012).
[22] A. C. Richardson, S. N. S. Reihani, and L. B. Oddershede, Opt. Express **16**, 15709 (2008).
[23] H. A. Kramers, Physica **7**, 284 (1940).
[24] A. Simon and A. Libchaber, Physica **68**, 3375 (1992).
[25] G. E. Crooks, Phys. Rev. E **60**, 2721 (1999).
[26] G. M. Wang, E. M. Sevick, E. Mittag, D. J. Searles, and D. J. Evans, Phys. Rev. Lett. **89**, 050601 (2002).
[27] D. Collin, F. Ritort, C. Jarzynski, S. B. Smith, I. Tinoco, and C. Bustamante, Nature (London) **437**, 231 (2005).
[28] V. Blickle, T. Speck, L. Helden, U. Seifert, and C. Bechinger, Phys. Rev. Lett. **96**, 070603 (2006).
[29] K. Sekimoto, *Stochastic Energetics*, Lecture Notes in Physics (Springer, Berlin/Heidelberg, 2010).
[30] G. Box, G. M. Jenkins, and G. Reinsel, *Time Series Analysis: Forecasting and Control*, 3rd ed. (Prentice Hall, Englewood Cliffs, NJ, 1994).
[31] O. Mazonka and C. Jarzynski, arXiv:cond-mat/9912121 (1999).
[32] G. Volpe and D. Petrov, Phys. Rev. Lett. **97**, 210603 (2006).
[33] U. Seifert, Phys. Rev. Lett. **95**, 040602 (2005).
[34] N. Goldenfeld, *Lectures on phase transitions and the renormalization group* (Addison-Wesley, Advanced Book Program, Reading, 1992) p. 226.
[35] M. Ibañes, J. García-Ojalvo, R. Toral, and J. M. Sancho, *Stochastic Processes in Physics, Chemistry, and Biology*, Lecture Notes in Physics, Vol. 557, edited by J. A. Freund and T. Pöschel (Springer-Verlag, Berlin, 2000), pp. 247–256.
[36] E. A. Novikov, Sov. Phys. JETP **20**, 1290 (1965).